

Draft version, August 9, 2002. Submitted to AJ.

Narrow-line Seyfert 1s from the SDSS Early Data Release

Rik J. Williams, Richard W. Pogge, and Smita Mathur

Department of Astronomy, The Ohio State University, Columbus, OH 43210-1173, USA

ABSTRACT

We present a sample of 150 narrow-line Seyfert 1s (NLS1s) found within the Sloan Digital Sky Survey Early Data Release (EDR), only one of which was previously identified as such. This more than triples the known number of NLS1s, and provides a basic method by which to identify many more with subsequent releases of SDSS data. With its large size and homogeneous, well-defined selection criteria, this sample will help alleviate two major problems which have plagued NLS1 research in the past; namely, their relative rarity (only ~ 60 objects previously identified) and significant differences in selection algorithms between the known samples. 45 of these SDSS-selected NLS1s are detected at energies of 0.1–2 keV in the ROSAT All-Sky Survey (RASS), and are found to have ultrasoft X-ray spectra with photon indices of $\Gamma \gtrsim 2$, in agreement with previous results for NLS1s. However, about 10–20 of those NLS1s that were not detected by ROSAT have optical properties very similar to the detected objects, and so should also have been detected by the RASS. This may be due to either significant intrinsic absorption in many NLS1s, or a significant sub-class of NLS1s that have uncharacteristic, intrinsically flatter (hence harder) X-ray spectral energy distributions.

Subject headings: galaxies: Seyfert—galaxies: active—X-rays: galaxies

1. Introduction

Since their initial classification by Osterbrock & Pogge (1985) narrow-line Seyfert 1s (NLS1s) have gained notoriety as interestingly extreme examples of active galactic nuclei (AGN). They were initially defined by their relatively narrow permitted emission lines ($\text{FWHM} \lesssim 2000 \text{ km s}^{-1}$; Goodrich 1989), strong Fe II relative to $\text{H}\beta$, and weak [O III]. In their analysis of 87 bright AGN, Boroson & Green (1992) found a strong anticorrelation between the strengths of the [O III] and Fe II lines (the primary correlation behind their so-called “Eigenvector 1” or “Principal Component 1”; PC1). NLS1s lie at the extreme, low-[O III] end of PC1. The authors suggested that this may be due to a high accretion rate relative to the Eddington rate. A more recent analysis by Boroson (2002) reinforces this claim, noting that NLS1s consistently exhibit the lowest estimated central black hole masses and the highest inferred relative accretion rates among the various AGN types.

Much attention has been devoted in recent years to the X-ray spectra of NLS1s. While AGN have long been known to emit a substantial fraction of their luminosity as X-rays, a soft X-ray “excess” was noted among Seyfert galaxies (e.g., Puchnarewicz et al. 1992, and references therein). Boller, Brandt, & Fink (1996) found a strong anticorrelation between the X-ray photon index (Γ , where $f_E \propto E^{-\Gamma}$) and $\text{FWHM}(\text{H}\beta)$, with NLS1s having $\Gamma \gtrsim 2.5$. Consequently, selection on the basis of ultrasoft X-ray emission has proven effective in the discovery of new NLS1s (Grupe 2000). This soft excess is thought to be the high-energy (Wien) tail of thermal emission from the inner accretion disk. Since extremely high temperatures are required to produce this emission, it again follows that NLS1s may be powered by low-mass black holes at high relative accretion rates (Pounds, Done, & Osborne 1995; Wang, Brinkmann & Bergeron 1996).

To date, a combination of X-ray and optical selection and serendipity (see Pogge 2000, for a review) has resulted in 64 catalogued NLS1s (Véron-Cetty, Véron, & Gonçalves 2001, hereafter VVG01). While these provide a starting point for studying the role of NLS1s among AGN phenomena, the sample size is relatively small and quite heterogeneous due to the wide variety of selection criteria employed. Since many known NLS1s were first discovered in X-rays, it is difficult to ascertain with confidence whether the extreme X-ray softness exhibited by most catalogued NLS1s is a fundamental property or a subtle selection effect. Clearly, a large and homogeneous optically selected sample would be advantageous in resolving these issues.

Such a sample is now becoming available in the form of the Sloan Digital Sky Survey (SDSS; York et al. 2000), in particular the Early Data Release (EDR; Stoughton et al. 2002), released in mid-2001. The EDR contains spectra of approximately 4000 quasars (Schneider et al. 2002) as well as a large number of Seyfert galaxies and other AGN. Photometric data are measured in five bands (u' , g' , r' , i' , and z' ; Fukugita et al. 1996), and criteria based on these bands are used to select QSO candidates for spectroscopic follow-up, as described in Richards et al. (2002). Parameters such as redshifts, magnitudes and linewidths are stored in a searchable database, with photometric properties in the “PhotoObj” class and spectral properties in the “SpecObj” and “SpecLine” classes. This database also has built into it an “ExternalCatalog” class, which contains all EDR objects within $60''$ of objects catalogued in the ROSAT All-Sky Survey (RASS), as well as some ROSAT-measured properties of these objects (see section 3.2).

By submitting a query restricted to objects with narrow $\text{H}\beta$ emission lines and then analyzing the resulting spectra, we have identified 150 NLS1s in the EDR, only one of which has been previously classified as such. In the following section we discuss in more detail the selection criteria and subsequent analysis. The overall selection methods and optical properties are discussed, as well as objects which were previously known and/or misidentified. Finally, we report on those objects which were also observed in RASS, and give possible reasons why some were not detected when they should have been.

2. Candidate selection from SDSS

Using the SDSS Query Tool¹, we searched for spectroscopically-targeted objects which were flagged as QSOs and which exhibited narrow H β lines. Velocity dispersions were estimated through the relation

$$\text{FWHM}(\text{H}\beta) = \frac{2.35c\sigma}{\lambda_0(1+z)} \quad (1)$$

where σ is the data member “sigma” in the SDSS SpecLine class, denoting the value of σ for a Gaussian curve fit to each H β line. To account for the possibility that the recorded dispersion estimates are subject to systematics, we initially relaxed the selection criteria, excluding only objects with $\text{FWHM}(\text{H}\beta) < 3000 \text{ km s}^{-1}$. The resulting 950 spectra were then visually inspected and measured to identify the NLS1s. Many of these spectra exhibited characteristics of Seyfert 1.5 and Seyfert 2 galaxies (strong [O III] compared to H β , no evidence of Fe II, obvious broad components H β and H α , etc.), while others were too faint or noisy to classify. All in all, this initial cut removed about half of the candidates from the sample.

The remaining objects generally exhibit the combination of narrow H β , strong Fe II and weak [O III] emission characteristic of NLS1s. Each spectrum was first transformed from the $\log(\lambda)$ space used by SDSS onto a linear wavelength scale and smoothed with a three-pixel boxcar filter. The smoothing step is analogous to that used in the EDR presentation spectra returned as .GIF files. We then performed a quadratic continuum fit near the H β line, measured its peak wavelength with a centroiding algorithm, and measured the width of the line halfway between the fitted continuum and the line peak. Since this method makes no assumptions about the underlying emission-line profile, we took this to be an accurate measurement of $\text{FWHM}(\text{H}\beta)$. All objects which exhibited a velocity dispersion larger than 2000 km s^{-1} , as well as those with evidence of a weak very broad component in H β or H α (when the latter was visible in the SDSS spectral band), were removed. The remaining 150 objects thus satisfy the Osterbrock & Pogge (1985) criteria and Goodrich (1989) FWHM cutoff, and comprise the NLS1 catalog presented here (see Table 1). Three of these NLS1 spectra are shown in figure 1, illustrating the spectral shape and appearance for various redshift and $\text{FWHM}(\text{H}\beta)$ regimes.

It is interesting to note the concordance between our measurements and those reported in the SDSS EDR database; namely, those of the redshift and H β linewidth. Figure 2 shows excellent agreement between the two redshift measurements with typical errors of 0.2% or less. Our redshift measurements are systematically higher by about 0.1%, but this is most likely due to properties of the H β line itself since we base this redshift only on H β , rather than on the narrow forbidden lines that are probably more representative of the systemic redshifts of the galaxies. When the most discrepant redshifts were re-measured using narrow forbidden lines (such as [O III] $\lambda 5007\text{\AA}$), our redshifts fall much more in line with the SDSS measurements. Since SDSS bases their redshift measurement on a cross-correlation between many lines and ours is only based on H β , we take the

¹Available from <http://archive.stsci.edu/sdss/software>

SDSS results to be the more accurate and definitive.

On the other hand, there are large discrepancies between our FWHM measurements and those estimated from the SDSS “sigma” parameter (see figure 3). Not only is there a significant amount of scatter, but our measurements are systematically lower than the SDSS estimates. Most of the scatter is probably caused by the $\sim 2\text{\AA}/\text{pixel}$ spectral resolution. That is, if our FWHM measurements vary intrinsically by ~ 2 pixels, this would correspond to an RMS variation of $\sim 250\text{ km s}^{-1}$, which is very close to the observed scatter.

The systematic offset is probably due to several factors. First, such a discrepancy is not particularly surprising since the SDSS FWHM is based on a Gaussian fit to a profile better represented by a Lorentzian or more complicated shape (see, for example, VVG01). These are compounded by the proximity of the Fe II complexes on either side of H β , which tends to drive the automatically-fitted continuum used by the SDSS analysis pipeline higher depending on the Fe II strength. In some cases, the line-fitting algorithm employed by SDSS appears to select only a broad component in the H β line, again giving larger FWHM values than our measurements. Thus, while SDSS measurements are quite useful for initial linewidth-based selection, careful follow-up measurements are absolutely necessary to take into account peculiarities in the individual spectra.

3. Sample properties

Table 1 lists the 150 objects which comprise this sample, along with various measured parameters and previous references to the catalogued objects, found through a NASA/IPAC Extragalactic Database (NED) query. Although 48 objects had been picked up in surveys such as 2dF, 2MASS, LBQS, and various other projects, most had not been formally classified as NLS1s. Of these, only one (SDSS J014644.82–004043.2) has been definitively identified as an NLS1 (VVG01). Puchnarewicz et al. (1992) list another (SDSS J011703.58+000027.4, also known as E0114–002) as a Seyfert 1 with $\text{FWHM}(\text{H}\beta) = 2980\text{ km s}^{-1}$, substantially higher than our measurement of 975 km s^{-1} ; however, the authors mention that this object’s H β line may be contaminated. Such contamination was not clearly seen in the SDSS spectrum, so we have included this object in our NLS1 sample. The remaining objects are listed in NED under such generic labels as “QSO,” “AGN,” or “Seyfert.” A few are flagged as “Sy1,” but it is unclear whether these were classified before OP85 first defined the NLS1 class. In the interest of brevity, Table 1 contains special references only to those objects flagged as some type of Seyfert galaxy in NED.

This sample thus represents 149 newly identified NLS1s, more than tripling the total number known. For $z < 0.5$ (where most of our objects lie), there are 135 objects in our sample out of 944 flagged as QSOs in the EDR. If we take this to be representative of the overall quasar population, this would imply that NLS1s make up roughly 15% of AGN at low redshifts. Until a more definitive selection of both NLS1s and QSOs is made from the SDSS, this number cannot be determined more than crudely. However, this is roughly consistent with the number quoted by Osterbrock (1987).

3.1. Constraints

The NLS1s we have found in the SDSS EDR span a range of redshifts from 0.04 to 0.75, the upper bound set by the requirement that $[\text{O III}] \lambda 5007 \text{\AA}$ not exceed the SDSS spectrograph limit of $\sim 9200 \text{\AA}$ (though in practice only three objects have $z > 0.6$). Although Schneider et al. (2002) warn that the quasar selection criteria are inhomogeneous for the EDR, the criteria for objects at these lower redshifts are actually quite well defined (Richards et al. 2002). Since NLS1s are identified primarily by the $\text{H}\beta$ velocity dispersion and the $[\text{O III}]$ and Fe II lines surrounding $\text{H}\beta$, we did not attempt to find NLS1-like AGN at redshifts beyond the range where $\text{H}\beta$ is seen. Furthermore, a search for narrow-lined objects in the SDSS Galaxy database yielded over 20,000 candidates, and thus it was not feasible to consider objects in that database with the selection methods described in this paper. By restricting ourselves to objects flagged as QSO, our sample also falls within the SDSS QSO color selection criteria described in Richards et al. (2002), making the basic selection very well understood. Even with these restrictions, there are enough objects to undertake a study of characteristics of this NLS1 sample.

3.2. X-ray properties

When these 150 objects are cross-referenced with the ROSAT All-Sky Survey catalogue (using an SDSS ExternalCatalog query), we find that 52 lie within $60''$ of X-ray detected sources. Power-law slopes were estimated using the ROSAT Hardness Ratio 1 parameter (HR1), which is defined as (Voges et al. 1999):

$$\text{HR1} = \frac{B - A}{B + A} \quad (2)$$

Here, A and B denote the number of counts in the 0.1–0.4 and 0.5–2.0 keV bands, respectively. Note that if there are zero counts in band A or B, HR1 becomes +1 or –1 respectively. By using HR1 and the sensitivity curve of ROSAT (as implemented in the PIMMS program²) and galactic N_H obtained from the “nh” utility³, it is possible to estimate the X-ray photon indices of ROSAT-detected NLS1s.

Of the 52 X-ray detected NLS1s in our sample, 7 have hardness ratios equal to (or within 1σ of) +1 or –1, with two in the former group and five in the latter. This may be indicative of extremely hard or soft X-ray spectra, respectively. However, these seven objects are all fairly faint in X-rays ($\lesssim 0.04 \text{ counts s}^{-1}$) and the two with $\text{HR1} = +1$ have unusually high galactic H I column densities; thus, it is unlikely that these seven objects have unusually hard or soft spectral energy distributions. Power-law slopes were estimated with PIMMS for the remaining 45 NLS1s

²Portable, Interactive Multi-Mission Simulator v3.2d, from NASA’s High Energy Astrophysics Science Archive Research Center (HEASARC), currently available at <http://heasarc.gsfc.nasa.gov/docs/software/tools/pimms.html>

³Part of the FTOOLS package, available at <http://heasarc.gsfc.nasa.gov/docs/software/ftools/>

and plotted against $\text{FWHM}(\text{H}\beta)$ (see figure 4). As in Boller et al. (1996), the photon indices of this sample of NLS1s span a range from approximately $2 \lesssim \Gamma \lesssim 4.5$ with little or no apparent dependence on the $\text{H}\beta$ linewidth. In particular, we note that the vast majority of these sources exhibit ultrasoft spectra with $\Gamma > 2$, as was seen in previous samples of soft X-ray selected NLS1s (e.g. Boller 2000, for a review).

Redshift and $g' - r'$ color distributions are shown in figures 5 and 6 respectively, with ROSAT-detected objects shown as the shaded portion of each histogram. Most of these RASS sources are optically bright ($g' \lesssim 18.5$); additionally, there appears to be a slight bias toward sources with lower redshifts and galactic H I column densities. Even with this taken into account by excluding objects with $N_H \geq 4 \times 10^{20} \text{ cm}^{-2}$, we still see several optically-bright, low redshift sources which should have been easily detected by RASS assuming similar spectral energy distributions, but which were not (see figure 7).

There are two likely interpretations for this. The first is that these undetected sources could have X-ray properties similar to the detected sources, but the soft X-rays are suppressed by a large ($N_H \gtrsim 10^{21} \text{ cm}^{-2}$) intrinsic column density. If this were the case, we would expect to see a pronounced difference in the spectral continuum shapes and/or the photometric colors between the X-ray detected and undetected objects; however, no such reddening is seen. The soft X-ray weak objects could be members of a gas-rich and dust-poor population (as proposed by Risaliti et al. 2001), which would account for the apparent lack of visual extinction, but this seems somewhat contrived.

The second possibility is that the undetected objects represent a new population of NLS1s with intrinsically flatter (and hence harder) X-ray slopes. In this case, the lack of soft X-rays would be due to a fundamental difference in the central black hole and accretion disk properties. For example, if these objects had larger black hole masses and high accretion rates, the accretion disk spectral energy distribution would shift to lower energies, effectively flattening out the 0.1–10 keV spectrum. Assuming similar spectral properties, these NLS1s would not have been detected in the RASS.

It should also be noted that strong X-ray variability could result in a significant fraction of NLS1s not detected by RASS. However, it is unlikely that such a large number of bright NLS1s would exhibit this degree of variability, and would coincidentally be X-ray faint at the time of observation by RASS. Whichever interpretation is correct, the X-ray undetected NLS1s are possibly something new and intriguing within NLS1 phenomena. Further X-ray observations of these NLS1s over a larger energy range with higher sensitivity may help to decipher the underlying cause of this observation.

4. Conclusions

The 150 SDSS-selected NLS1s presented in this paper represent more than a threefold increase in the total known number of these extreme AGN. They comprise approximately 15% of the EDR “QSO” database at $z \lesssim 0.5$ and have very well-defined color and linewidth selection criteria. 45 of these NLS1s were also detected with good confidence in the 0.1–2 keV band of the ROSAT All-Sky Survey and exhibit ultrasoft X-ray spectra. Of the NLS1s that were *not* detected, several have similar optical properties to NLS1s seen in the RASS, and thus should have been detected as well. This may be due to either high intrinsic absorption or harder X-ray spectra (or both) among the undetected objects. More optical and X-ray data will almost certainly be helpful in determining the cause behind this.

It should also be noted that while most of our objects clearly fall within the defining NLS1 criteria, a substantial fraction are near the 2000 km s^{-1} FWHM cutoff. Additionally, several of the spectra had low signal-to-noise ratios. This may hide characteristics (such as a broad component in $H\beta$) which would reclassify the object as a Seyfert 1.5 or other type. While these objects all appear to be NLS1s from the data given, it is likely that some may be reclassified when higher resolution, higher signal-to-noise spectra are obtained. Thus, this sample should be considered a list of very strong NLS1 candidates rather than a definitive list. Nevertheless, this sample has shown that large numbers of NLS1s (and other interesting objects) can indeed be selected from the SDSS Early Data Release. Since the EDR represents only about 5% of the total spectroscopic survey (Stoughton et al. 2002), future releases will prove indispensable for further discoveries and study of NLS1s.

The authors would like to thank David Weinberg for helpful discussions. RJW acknowledges support from an OSU University Fellowship. SM is supported by Chandra X-ray Observatory grant G01-2118X from Smithsonian Astrophysical Observatory.

Funding for the creation and distribution of the SDSS Archive has been provided by the Alfred P. Sloan Foundation, the Participating Institutions, the National Aeronautics and Space Administration, the National Science Foundation, the U.S. Department of Energy, the Japanese Monbukagakusho, and the Max Planck Society. The SDSS Web site is <http://www.sdss.org/>.

The SDSS is managed by the Astrophysical Research Consortium (ARC) for the Participating Institutions. The Participating Institutions are The University of Chicago, Fermilab, the Institute for Advanced Study, the Japan Participation Group, The Johns Hopkins University, Los Alamos National Laboratory, the Max-Planck-Institute for Astronomy (MPIA), the Max-Planck-Institute for Astrophysics (MPA), New Mexico State University, Princeton University, the United States Naval Observatory, and the University of Washington.

This research has made use of the NASA/IPAC Extragalactic Database (NED) which is operated by the Jet Propulsion Laboratory, California Institute of Technology, under contract with the

National Aeronautics and Space Administration.

REFERENCES

- Boller, Th. 2000, *NewAR*, 44, 387
- Boller, Th., Brandt, W. N., & Fink, H. 1996, *A&A*, 305, 53
- Boroson, T. A. 2002, *ApJ*, 565, 78
- Boroson, T. A. & Green, R. F. 1992, *ApJS*, 80, 109
- Fukugita, M., Ichikawa, T., Gunn, J. E., Doi, M., Shimasaku, K., & Schneider, D. P. 1996, *AJ*, 111, 1748
- Goodrich, R.W. 1989, *ApJ*, 342, 234
- Grupe, D. 2000, *NewAR*, 44, 455
- La Franca, F., Cristiani, S., & Barbieri, C. 1992, *AJ*, 103, 1062
- Osterbrock, D. E. 1987, *Lecture Notes in Physics 307*, Springer Verlag, Heidelberg, p. 1
- Osterbrock, D. E. & Pogge, R. W. 1985, *ApJ*, 297, 166
- Pogge, R. W. 2000, *NewAR*, 44, 381
- Pounds, K. A., Done, C., & Osborne, J. P. 1995, *MNRAS*, 277, L5
- Puchnarewicz, E. M., Mason, K. O., Córdova, F. A., Kartje, J., Branduardi-Raymont, G., Mittaz, J. P. D., Murdin, P. G., & Allington-Smith, J. 1992, *MNRAS*, 256, 589
- Richards, G. T., et al. 2002, *AJ*, 123, 2945
- Risaliti, G., Marconi, A., Maiolino, R., Salvati, M., & Severgnini, P. 2001, *A&A*, 371, 37
- Schneider, D. P., et al. 2002, *AJ*, 123, 567
- Stephens, S. A. 1989, *AJ*, 97, 10
- Stoughton, C., et al. 2002, *AJ*, 123, 485
- Véron-Cetty, M.-P. & Véron, P. 2001, *A&A*, 374, 92
- Véron-Cetty, M.-P., Véron, P., & Gonçalves, A. C. 2001, *A&A*, 372, 730
- Voges, W., et al. 1999, *A&A*, 349, 389
- Wang, T., Brinkmann, W., & Bergeron, J. 1996, *A&A*, 309, 81

York, D. G., Adelman, J., Anderson, J.E., et al. 2000, AJ, 120, 1579

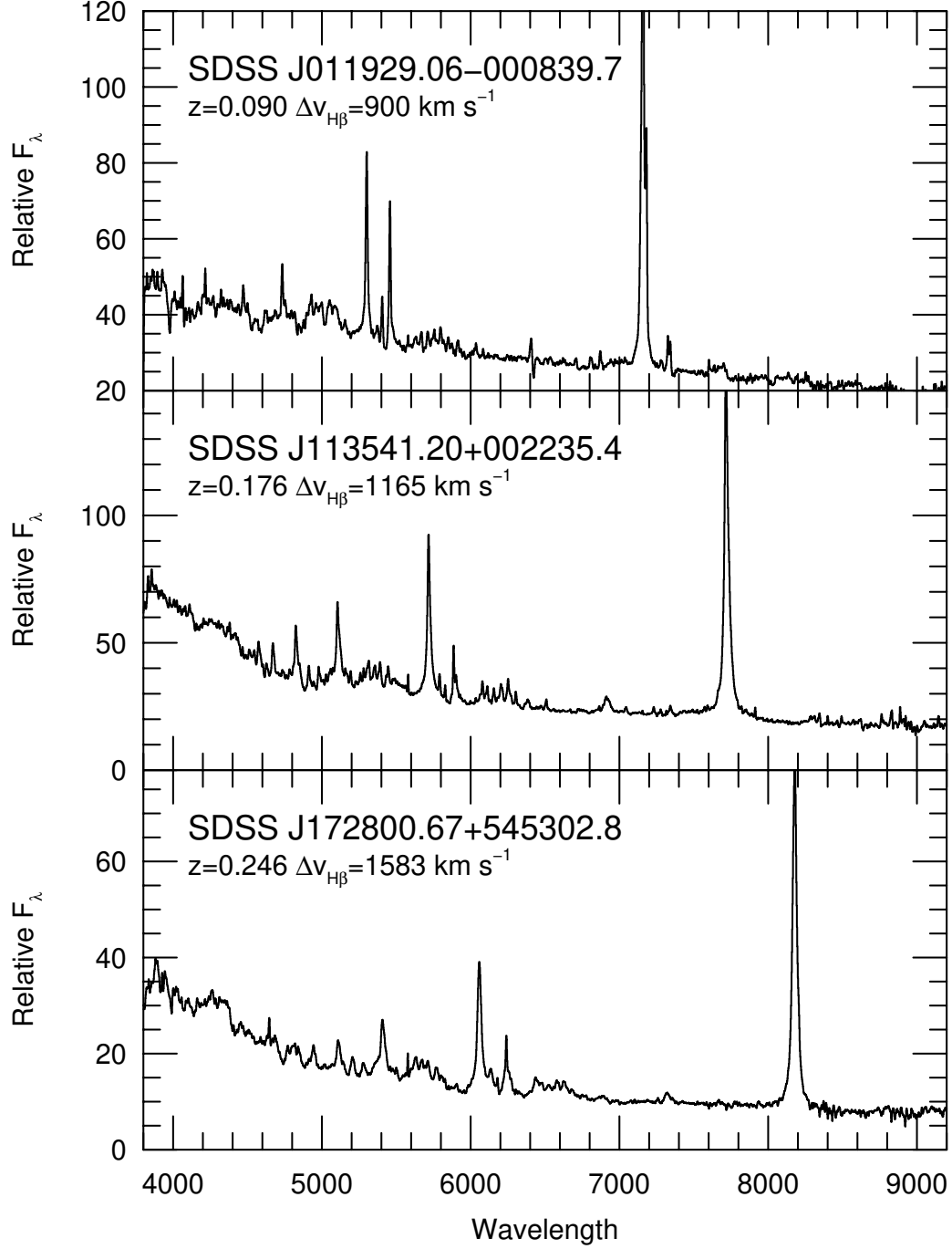


Fig. 1.— Examples of three spectra from the NLS1 sample described in this paper, taken from different FWHM($H\beta$) and redshift regimes.

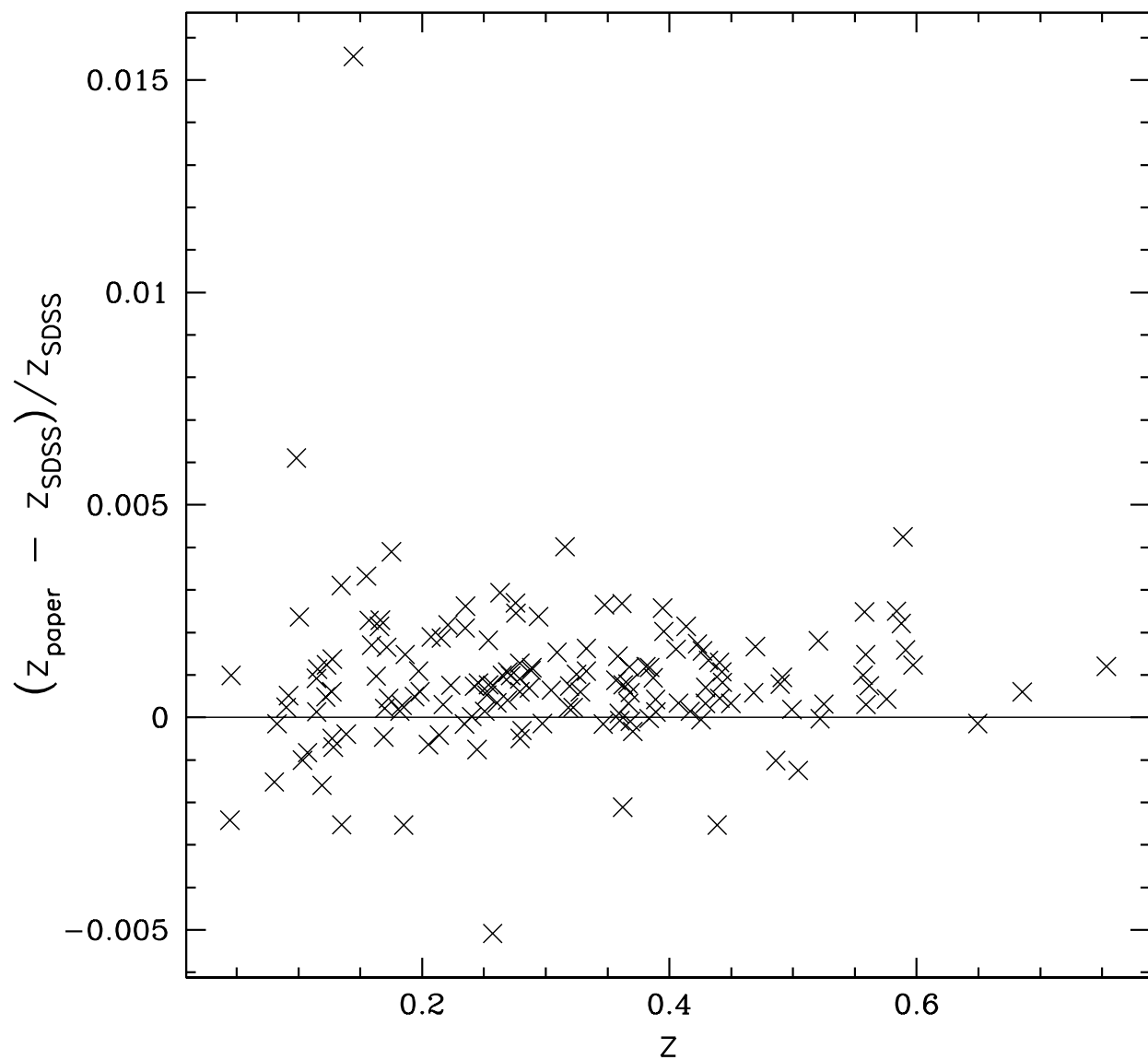


Fig. 2.— Fractional differences between our redshift measurements and those made by SDSS.

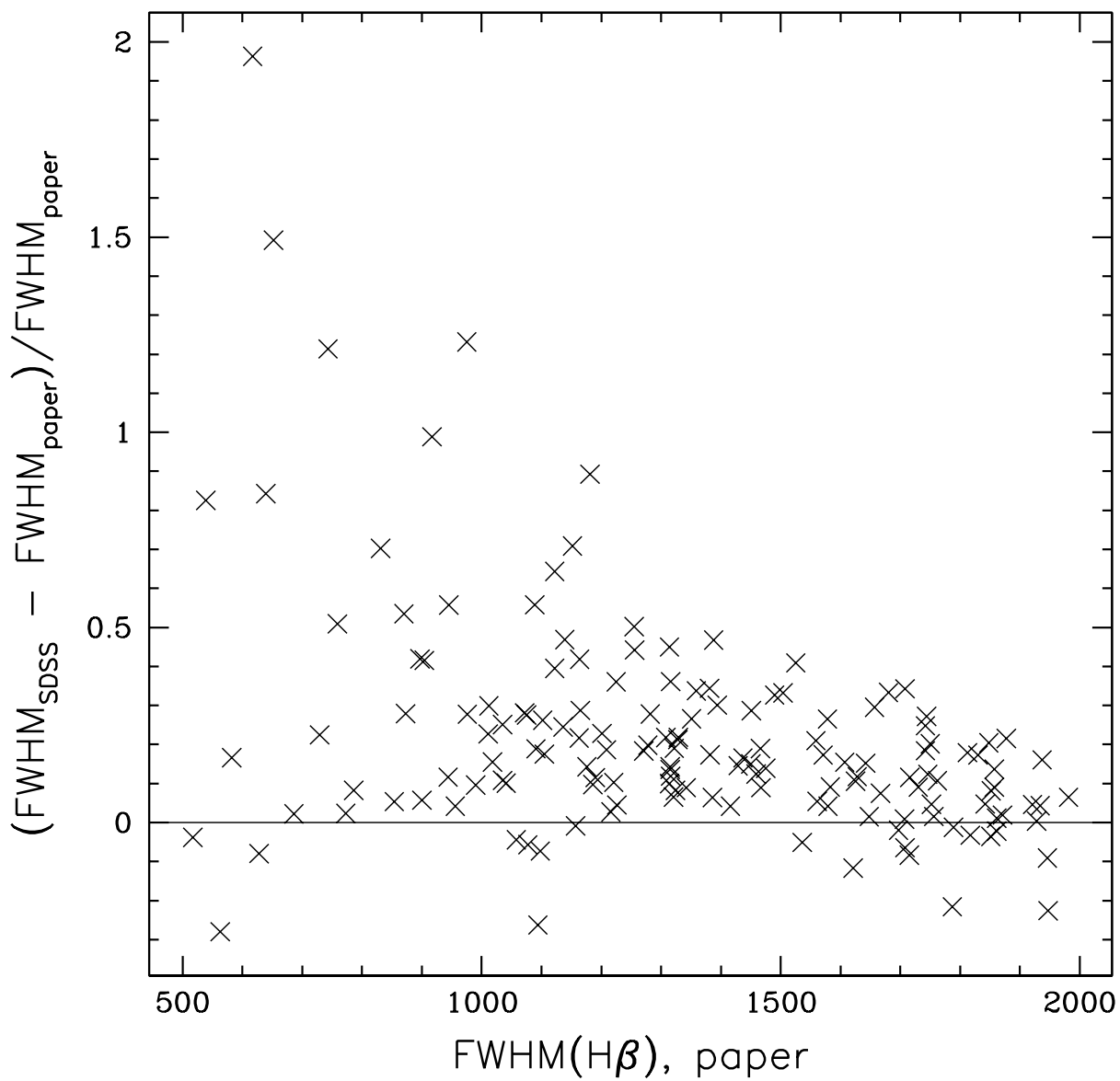


Fig. 3.— Fractional differences between our FWHM measurements and those made by SDSS.

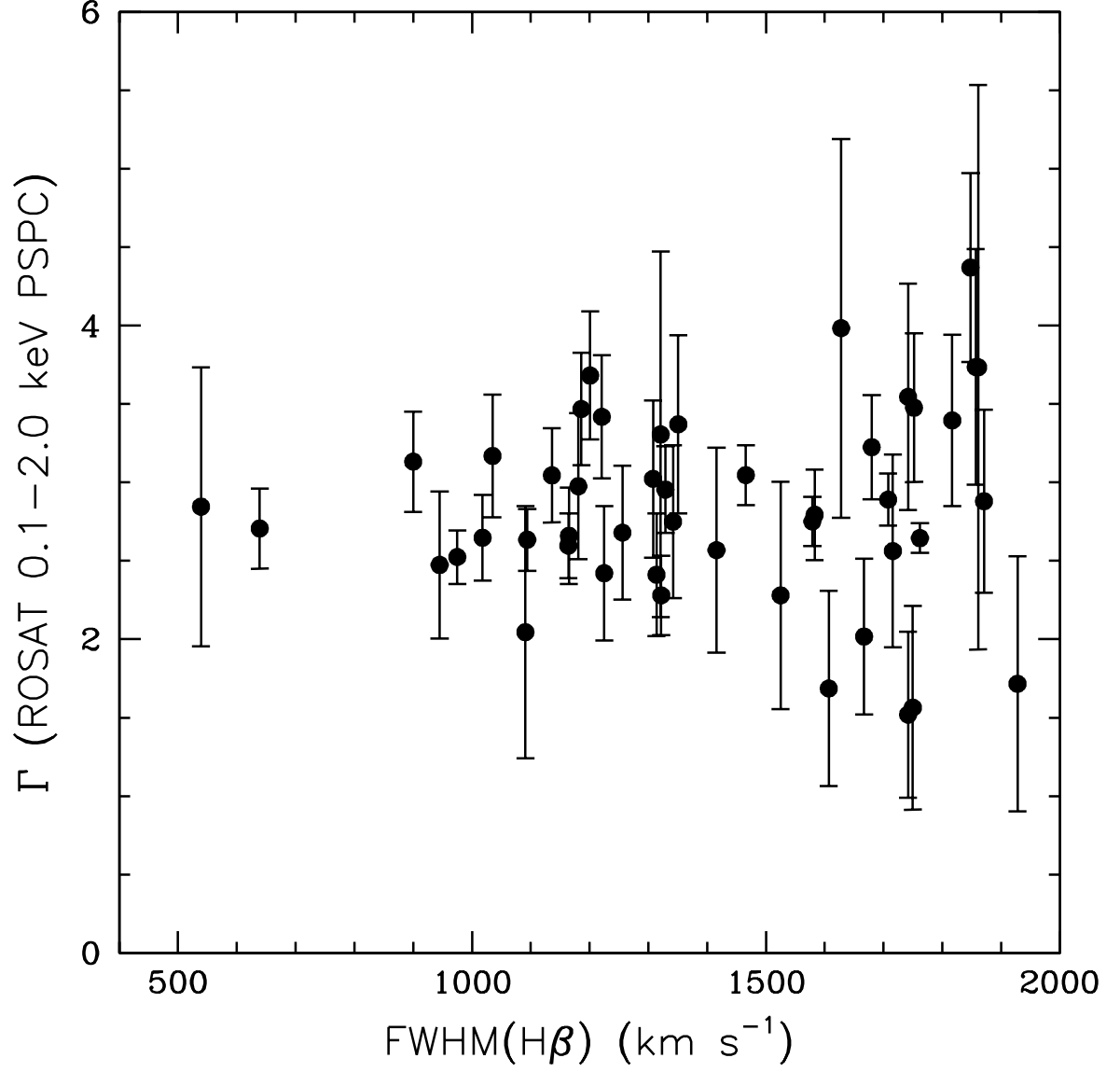


Fig. 4.— Photon index vs. $H\beta$ velocity dispersion for the ROSAT-detected NLS1s.

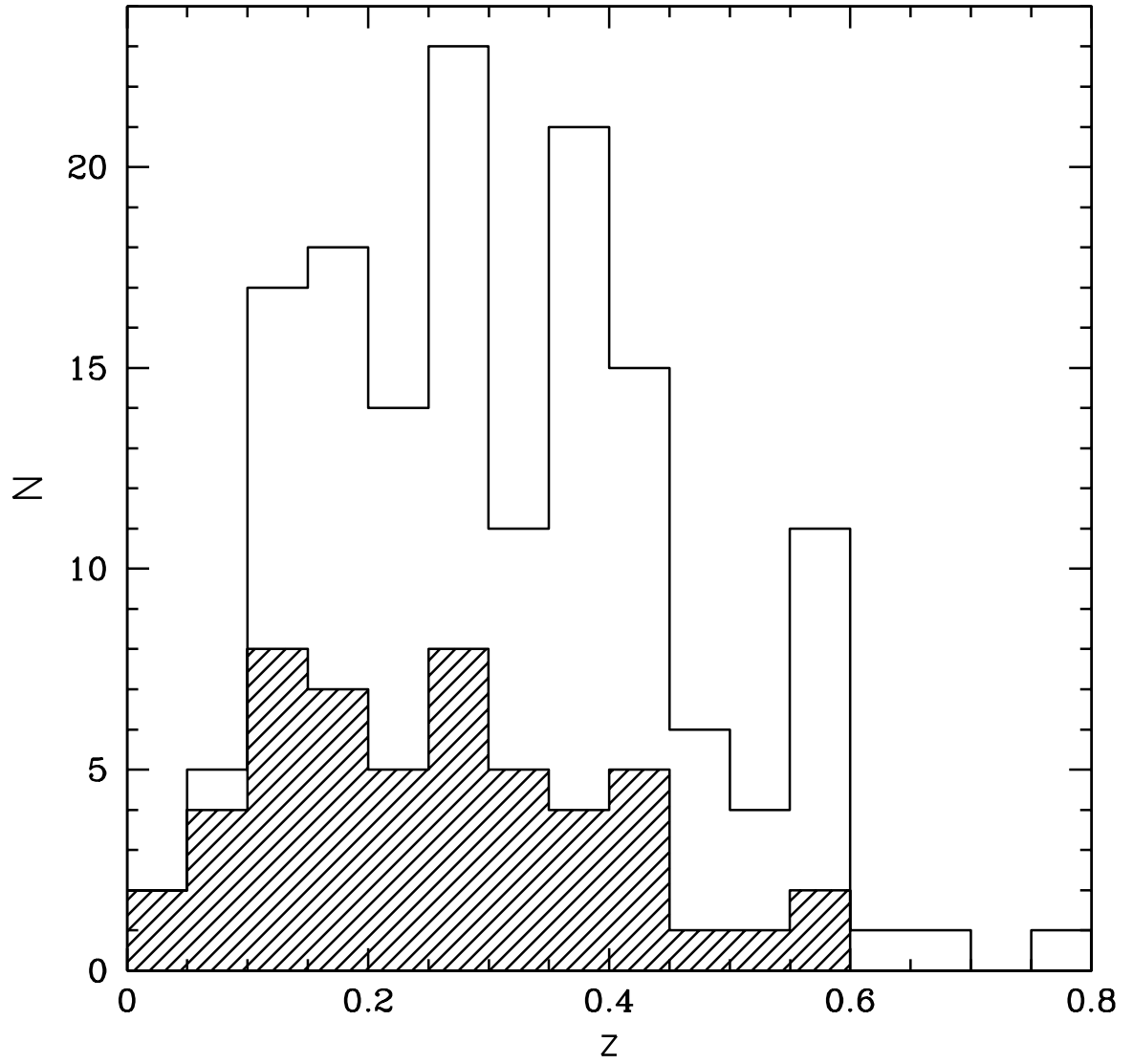


Fig. 5.— Redshift distribution for this NLS1 sample. ROSAT-detected NLS1s are shown as the shaded portion of the histogram.

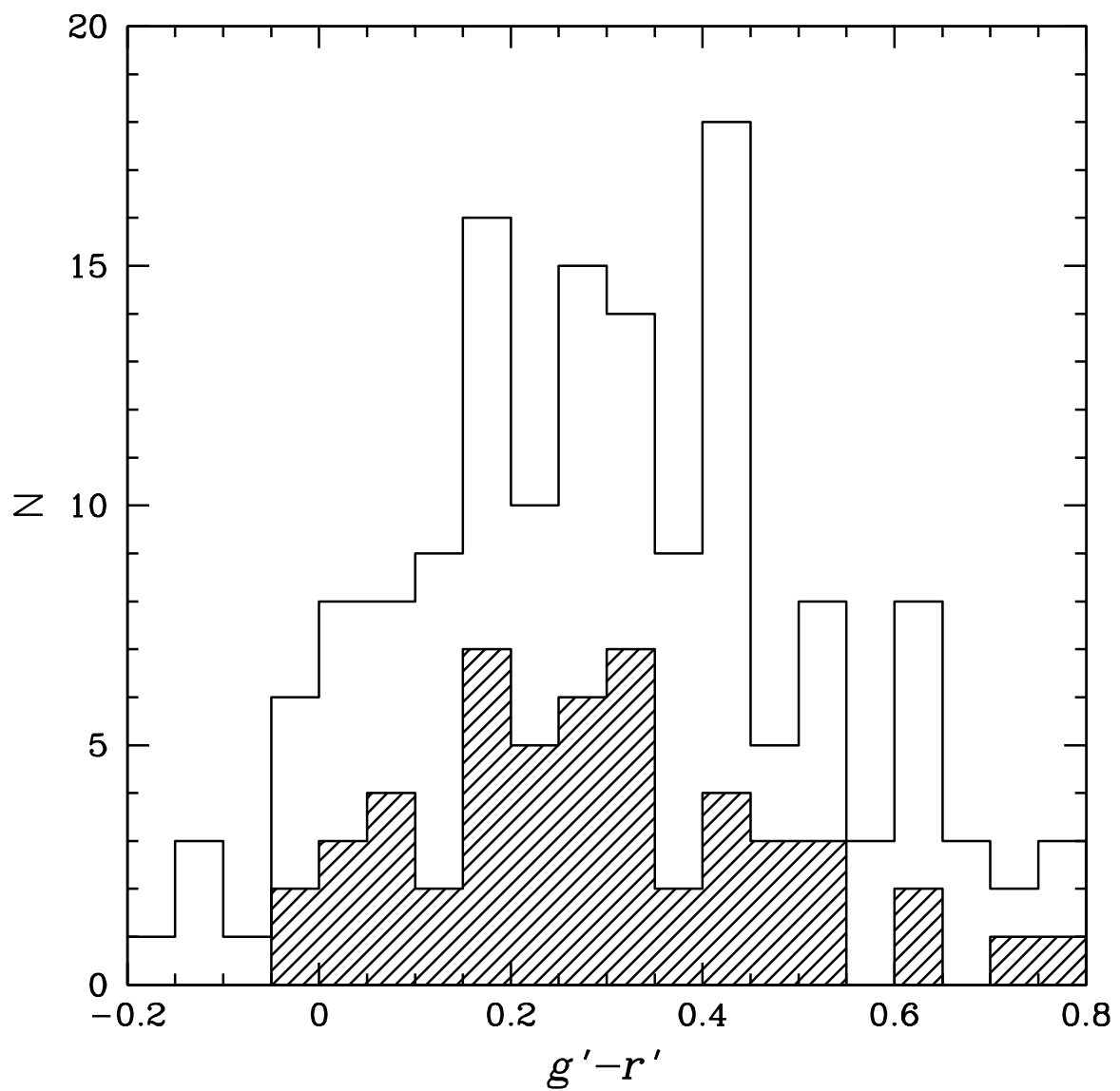


Fig. 6.— SDSS $g' - r'$ color distribution for this NLS1 sample. ROSAT-detected NLS1s are shown as the shaded portion of the histogram.

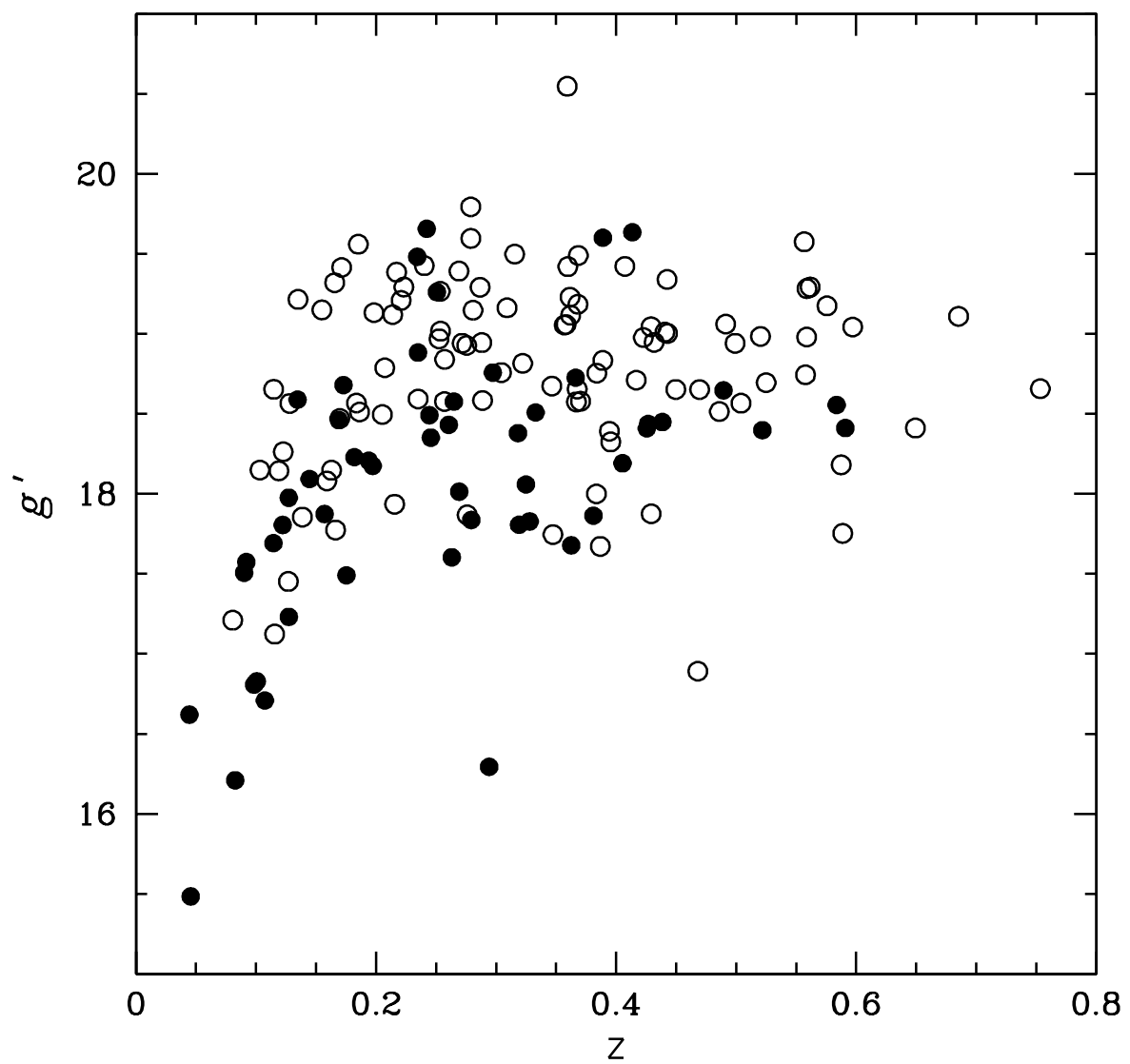


Fig. 7.— Magnitude-redshift relation for this sample. Filled circles denote those objects detected in the ROSAT All-Sky Survey, while open circles were not detected.

Table 1. NLS1s from the SDSS Early Data Release

SDSS Name ^a	z	FWHM(H β)	HR1	Γ	Notes
J000109.14-004121.5	0.417	1209
J000834.72+003156.2	0.263	1351	-0.46 ± 0.29	3.4 ± 0.6	...
J001327.31+005232.0	0.363	1742	-0.57 ± 0.31	3.5 ± 0.7	...
J002213.00-004832.7	0.214	1429
J002233.27-003448.6	0.504	1388
J002305.03-010743.5	0.166	1157
J002752.39+002615.8	0.205	1830
J003024.94+000254.5	0.288	743
J003238.20-010035.2	0.092	639	-0.10 ± 0.17	2.7 ± 0.3	...
J003431.74-001312.7	0.381	1314	0.03 ± 0.27	2.4 ± 0.4	...
J003711.00+002128.0	0.235	617
J004052.14+000057.3	0.405	1278
J004338.54-005814.7	0.559	1122
J005446.16+004204.1	0.234	1225	0.09 ± 0.29	2.4 ± 0.4	...
J005921.37+004108.9	0.423	1625
J010226.31-003904.6	0.294	1680	-0.24 ± 0.20	3.2 ± 0.3	...
J011357.93-011139.8	0.754	1842
J011703.58+000027.4	0.046	975	0.20 ± 0.11	2.5 ± 0.2	1
J011712.81-005817.5	0.486	1937
J011929.06-000839.7	0.090	900	-0.22 ± 0.20	3.1 ± 0.3	2
J013046.16-000800.8	0.253	1648
J013521.68-004402.2	0.098	1181	-0.23 ± 0.29	3.0 ± 0.5	...
J013842.05+004020.0	0.520	1035
J013940.99-010944.4	0.194	1091	0.36 ± 0.49	2.0 ± 0.8	...
J014234.41-011417.4	0.244	1607	0.55 ± 0.31	1.7 ± 0.6	...
J014412.77-000610.5	0.359	1041
J014542.78+005314.9	0.389	1255
J014559.45+003524.7	0.166	1075
J014644.82-004043.2	0.083	1164	0.00 ± 0.14	2.6 ± 0.2	3
J014951.66+002536.5	0.252	563
J015249.76+002314.7	0.589	1852
J015652.43-001222.0	0.163	1324
J020431.64+002400.5	0.171	1077

Table 1—Continued

SDSS Name ^a	z	FWHM(H β)	HR1	Γ	Notes
J021610.56+000538.4	0.384	1467
J021652.47-002335.3	0.304	854
J022205.37-004948.0	0.525	1571
J022756.28+005733.1	0.128	773
J022841.48+005208.6	0.186	990
J022923.43-000047.9	0.558	1386
J023057.39-010033.7	0.649	1947
J023211.83+000802.4	0.432	1746
J023414.58+005707.9	0.269	1381
J024037.89+001118.9	0.470	1789
J024651.91-005931.0	0.468	1504
J025501.19+001745.5	0.360	904
J030031.31+005357.2	0.198	1536	4
J030417.78+002827.4	0.044	1321	0.46 ± 0.39	3.3 ± 1.2	...
J030639.57+000343.2	0.107	1525	0.80 ± 0.17	2.3 ± 0.7	...
J031427.47-011152.4	0.387	1812
J031542.64+001228.7	0.207	870
J031630.79-010303.6	0.368	1226
J032255.49+001859.9	0.384	1621
J032337.65+003555.7	0.215	1490
J032606.75+011429.9	0.127	686
J033027.21+005433.7	0.443	1315
J033059.06+010952.1	0.557	1946
J033429.44+000611.0	0.347	1316
J033854.25+005339.7	0.279	1314
J033923.66-002310.3	0.369	1437
J034131.95-000933.0	0.223	897
J034326.51+003915.2	0.499	1315
J034430.03-005842.7	0.287	786
J094857.33+002225.5	0.584	1342	0.31 ± 0.27	2.8 ± 0.5	...
J095859.80+004718.9	0.235	1190
J100405.00-003253.4	0.289	582
J101314.86-005233.5	0.276	1578

Table 1—Continued

SDSS Name ^a	z	FWHM(H β)	HR1	Γ	Notes
J102059.72+010034.3	0.588	1715
J102450.52-002102.4	0.322	1382
J103031.41-001902.6	0.562	1787
J103222.58-000345.6	0.559	1707
J103457.29-010209.0	0.328	1394
J104132.35-003512.2	0.135	1316
J104210.03-001814.7	0.115	628
J104230.14+010223.7	0.116	1012
J104331.51-010732.9	0.362	1756
J104449.28+000301.2	0.443	1176
J105932.52-004354.7	0.155	1451
J110312.83+000012.5	0.276	1450
J111022.39-005544.5	0.257	1934
J111307.73+003210.4	0.346	976
J113102.28-010122.0	0.242	1928	0.60 ± 0.37	1.7 ± 0.8	...
J113541.20+002235.4	0.175	1165	-0.16 ± 0.20	2.7 ± 0.3	2
J115023.59+000839.1	0.127	1136	-0.45 ± 0.16	3.0 ± 0.3	2
J115306.95-004512.7	0.357	1102
J115412.77+010133.4	0.490	945	-0.11 ± 0.32	2.5 ± 0.5	...
J115533.50+010730.6	0.197	1628	-0.81 ± 0.26	4.0 ± 1.2	...
J115755.47+001704.0	0.261	1762	-0.24 ± 0.29	2.6 ± 0.1	...
J115832.81+005139.2	0.591	1035	-0.55 ± 0.18	3.2 ± 0.4	...
J121415.17+005511.4	0.396	1981
J122102.95-000733.7	0.366	517
J122432.40-002731.4	0.157	1308	-0.48 ± 0.26	3.0 ± 0.5	...
J124519.73-005230.4	0.221	1730
J125337.36-004809.6	0.427	1416	-0.35 ± 0.39	2.6 ± 0.7	...
J125943.59+010255.1	0.394	1459
J130023.22-005429.8	0.122	1018	-0.40 ± 0.16	2.6 ± 0.3	...
J130707.71-002542.9	0.450	1475
J130855.18+004504.1	0.429	1851
J131108.48+003151.8	0.429	1642
J132231.13-001124.5	0.173	1861	-0.78 ± 0.45	3.7 ± 1.8	...

Table 1—Continued

SDSS Name ^a	z	FWHM(H β)	HR1	Γ	Notes
J133031.41-002818.8	0.240	1216
J133741.76-005548.2	0.279	873
J135908.01+002732.0	0.257	1282
J141234.68-003500.0	0.127	1098
J141519.50-003021.6	0.135	1186	-0.46 ± 0.18	3.5 ± 0.4	...
J141820.33-005953.7	0.254	831
J142441.21-000727.1	0.318	1201	-0.58 ± 0.17	3.7 ± 0.4	...
J143030.22-001115.1	0.103	1744
J143230.99-005228.9	0.362	1559
J143624.82-002905.3	0.325	1857	-0.54 ± 0.33	3.7 ± 0.8	...
J144735.25-003230.5	0.217	1105
J144913.51+002406.9	0.441	944
J144932.70+002236.3	0.081	1072
J145123.02-000625.9	0.139	1122
J145437.84-003706.6	0.576	1328
J150629.23+003543.2	0.370	1861
J151312.41+001937.5	0.159	1697
J151956.57+001614.6	0.115	1716	0.40 ± 0.34	2.6 ± 0.6	...
J153243.67-004342.5	0.309	1877
J153911.17+002600.8	0.265	539	0.46 ± 0.45	2.8 ± 0.9	...
J164907.64+642422.3	0.184	759
J165022.88+642136.1	0.407	1152
J165338.69+634010.7	0.279	1848	-0.83 ± 0.11	4.4 ± 0.6	...
J165537.78+624739.0	0.597	1271
J165633.87+641043.7	0.272	1139
J165658.38+630051.1	0.169	1466	-0.35 ± 0.11	3.0 ± 0.2	...
J165905.45+633923.6	0.368	1359
J170546.91+631059.1	0.119	1657
J170812.29+601512.6	0.145	1094	-0.16 ± 0.13	2.6 ± 0.2	...
J170956.02+573225.5	0.522	1329	-0.36 ± 0.16	3.0 ± 0.3	...
J171033.21+584456.8	0.281	652
J171207.44+584754.5	0.269	1708	-0.34 ± 0.10	2.9 ± 0.2	...
J171540.92+560655.0	0.297	1752	-0.56 ± 0.21	3.5 ± 0.5	...

Table 1—Continued

SDSS Name ^a	z	FWHM(H β)	HR1	Γ	Notes
J171829.01+573422.4	0.101	1322	0.16 ± 0.17	2.3 ± 0.3	...
J172007.96+561710.7	0.389	1221	-0.47 ± 0.20	3.4 ± 0.4	...
J172206.04+565451.6	0.426	1579	-0.07 ± 0.10	2.8 ± 0.2	...
J172756.86+581206.0	0.414	1742	0.65 ± 0.22	1.5 ± 0.5	...
J172800.67+545302.8	0.246	1583	-0.06 ± 0.19	2.8 ± 0.3	...
J172823.61+630933.9	0.439	1750	0.61 ± 0.29	1.6 ± 0.6	...
J173404.85+542355.1	0.685	1163
J173721.14+550321.7	0.333	1256	0.11 ± 0.28	2.7 ± 0.4	...
J232525.53+001136.9	0.491	1921
J233032.95+000026.4	0.123	956
J233149.49+000719.5	0.367	1708
J233853.83+004812.4	0.170	1011
J234050.53+010635.6	0.358	729
J234141.50-003806.7	0.319	1871	0.00 ± 0.38	2.9 ± 0.6	...
J234150.81-004329.2	0.251	1817	-0.32 ± 0.31	3.4 ± 0.5	...
J234216.74+000224.1	0.185	917
J234229.46-004731.6	0.316	1857
J234725.30-010643.7	0.182	1667	0.52 ± 0.25	2.0 ± 0.5	...

^aFormat: SDSS JHHMMSS.ss \pm DDMMSS.s

Note. — (1) Previously classified as a Seyfert 1 by Puchnarewicz et al. (1992); (2) Listed as a Seyfert 1 in NED, due to reference in Véron-Cetty & Véron (2001); (3) Previously listed as a NLS1 in VVG01; (4) Listed as a Seyfert galaxy in La Franca, Cristiani, & Barbieri (1992)